Response of traveling waves to transient inputs in neural fields

Zachary P. Kilpatrick* and Bard Ermentrout
Department of Mathematics, University of Pittsburgh, Pittsburgh, Pennsylvania 15260, USA
(Received 15 November 2011; revised manuscript received 22 January 2012; published 14 February 2012)

We analyze the effects of transient stimulation on traveling waves in neural field equations. Neural fields are modeled as integro-differential equations whose convolution term represents the synaptic connections of a spatially extended neuronal network. The adjoint of the linearized wave equation can be used to identify how a particular input will shift the location of a traveling wave. This wave response function is analogous to the phase response curve of limit cycle oscillators. For traveling fronts in an excitatory network, the sign of the shift depends solely on the sign of the transient input. A complementary estimate of the effective shift is derived using an equation for the time-dependent speed of the perturbed front. Traveling pulses are analyzed in an asymmetric lateral inhibitory network and they can be advanced or delayed, depending on the position of spatially localized transient inputs. We also develop bounds on the amplitude of transient input necessary to terminate traveling pulses, based on the global bifurcation structure of the neural field.

DOI: 10.1103/PhysRevE.85.021910 PACS number(s): 87.19.lq, 87.10.Ed, 87.19.lj, 87.19.lr

I. INTRODUCTION

Spatially structured activity in large neuronal populations subserves a number of functional and pathological events in the brain [1]. In particular, traveling waves of electrical activity have been observed in various sensory and motor areas [2]. Sensory inputs have been shown to initiate such events in olfactory [3] and visual [4] cortical regions. However, it is not clear whether such waves are a means of reloading the network for novel stimuli or propagating the signal to other portions of cortex [5]. There is evidence to suggest that waves of cortical activity may serve as a "spotlight" searching for novel stimuli, so the spatiotemporal location of an arriving stimulus can be encoded by the phase of the wave [6]. The preparation of motor commands has also been shown to correlate with the formation of propagating waves in the primate motor cortex [7]. In particular, the latency and amplitude of evoked waves appear to encode information regarding the target of motion. The spatial organization of neural populations can also be hijacked by pathological events such as propagated activity during epileptic seizures [8]. One particular epilepsy hypothesis, presuming there is some unhindered excitation in seizure-prone regions, has been explored using *in vitro* studies of disinhibited cortical slices [9]. Such paradigms have been very useful for probing how external stimuli can initiate [10] and modulate [11] traveling electrical waves.

Neural field models of large-scale cortical populations have been quite successful at providing a theory regarding the formation of traveling waves of neural activity [12,13]. A seminal study by Wilson and Cowan, introducing a system describing average activity of a spatially organized network, showed that a combination of excitation and inhibition can generate traveling pulses of activity [14]. Amari was then able to analytically treat a version of this model under the assumption that the firing rate nonlinearity in the system was a Heaviside function [15]. Analogous systems have been shown to support a number of spatiotemporal solutions such as patterns reminiscent of hallucinations [16,17], traveling fronts [18–20], traveling pulses [21], and stationary pulses [22]. One additional detail to consider is the effects of finite axonal conduction velocities by including delay terms in the evolution equations [21,23,24]. Also, negative feedback processes such as synaptic depression and spike frequency adaptation have been introduced in some neural field models as auxiliary variables [12,21,25,26]. These systems admit more exotic behaviors such as self-sustained oscillations [26,27], breathers emerging in the presence [28] or absence [29] of stimuli, and spiral waves [30]. A wide variety of spatiotemporal solutions arise in neural field equations in the absence of external inputs.

Persistent inputs have been shown to generate behavior not present in the associated unstimulated neural field. For moving inputs, stimulus-locked traveling waves can undergo a Hopf bifurcation beyond which traveling breathers exist [31,32]. Pulsating fronts can arise when a spatially periodic stationary input is applied [33]. These results echo experimental findings that show that external electric fields can modulate the speed of traveling waves in cortical slice experiments [11]. Recently, it was shown that spatially homogeneous time-periodic inputs give rise to hexagonal or rectangular patterns, depending on the period of the input [34], successfully describing psychophysical experiments regarding flicker phosphenes [35]. Few studies have spoken to the potential effects of transient stimuli on spatiotemporal dynamics of neural fields [24]. In Ref. [23] it was shown numerically that they can be used to remove topological defects from patterned activity. Experimentally, transient stimuli have been shown to functionally manipulate coherent neural activity [3,4] and may even serve to terminate pathological waves present during epileptic seizures [36]. With the advent of recent optogenetic techniques for abruptly manipulating the activity of populations of neurons [37], it seems likely that the effect of transient stimuli on spatiotemporal dynamics could be studied in a variety of *in vitro* and *in vivo* contexts.

Thus, we propose to analyze the effects of transient stimuli on coherent activity in neural field models. Our analytical framework extends previous numerical studies of transient stimuli in neural fields [23,24] and makes use of the zero eigenmode of the adjoint as a response function for spatially extended systems [20,38,39]. In particular, we study how the

*zpkilpat@pitt.edu

speed and location of traveling waves are affected since such analyses could likely be experimentally testable [11]. Some of our results even speak to the critical stimuli necessary to terminate traveling waves. The stimulus, in our models, represents a short input of current from an electrode [10], rapid alteration of an external electric field [11], or a brief activation of cells with light-sensitive ion channels [37]. Parts of our theory apply to large-amplitude stimuli, capable of switching parts of the network on or off.

The paper is organized as follows. In Sec. II we introduce a general neural field model that supports traveling fronts and/or pulses. For transparency, we analyze some of the simplest systems that produce a particular dynamical behavior. However, our results can be extended to more intricate models too. In Sec. III we analyze an excitatory neural field equation that supports traveling fronts. By deriving an effective response function, we can quantify the distance a front is advanced or delayed as it depends on the amplitude and form of a transient stimulus. In Sec. IV we analyze a spatially periodic neural field with an asymmetric lateral inhibitory weight kernel that supports traveling pulses. Extending our analysis for fronts, we quantify the delays or advances of the pulse to a spatially localized input and derive the response function in the same way. Fronts in the excitatory network can only be advanced by local positive perturbations while pulses in a lateral inhibitory network can be advanced or delayed, depending on the spatial location of the perturbation. Considering the bifurcation structure of the system, we can also calculate the critical inhibitory stimulus necessary to terminate the pulse.

II. SCALAR NEURAL FIELD MODELS

Perhaps the simplest neural field model that admits spatiotemporally patterned activity is the one-dimensional scalar model [15]

$$u_t = -u + \int_{-l}^{l} w(x-y) f[u(y,t)]dy + I(x,t), \qquad (1)$$

where $u(x,t)$ represents the sum of synaptic inputs to position x at time t [13]. For the purposes of a transparent exposition, we ignore the effects of finite axonal conduction velocities [21,23,24] and local negative feedback [12,21,25,26]. Spatial domains are often taken to be the real line, so that $l \to \infty$ [18], but some studies have also addressed periodic domains where $l = \pi$ [25]. The strength of synaptic weights from neurons at position y to neurons at x is encoded by the kernel $w(x-y)$. While $w(x)$ is often considered to be an even function, it does not have to be. For our studies of traveling fronts (where $l = \infty$), we consider the exponential weight function

$$w(x) = \tfrac{1}{2} e^{-|x|}. \qquad (2)$$

However, in our analysis of the periodic asymmetric network (where $l = \pi$), we consider the shifted cosine weight function

$$w(x) = A\cos(x-\phi), \qquad (3)$$

with amplitude A, where ϕ introduces a shift to the even cosine function. A similar weight kernel was considered in a study of directionally selective networks of visual cortex [40] and there are several experimental studies supporting the existence of functionally specific asymmetries in the spatial organization of synaptic inputs [41–43]. The nonlinearity $f(u)$ represents the relationship between the synaptic input and the output firing rate. Saturating sigmoid functions are often considered as appropriate representations of this firing rate function

$$f(u) = \frac{1}{1+e^{-\gamma(u-\theta)}}, \qquad (4)$$

where γ and θ are the gain and threshold of the firing rate function. In order to derive analytical results for our studies of traveling waves, it is often useful to consider the high-gain limit $\gamma \to \infty$ of Eq. (4) and employ a Heaviside firing rate function [12,13]

$$f(u) = H(u-\theta) = \begin{cases} 1, & u > \theta \\ 0, & u < \theta. \end{cases} \qquad (5)$$

This mathematical convenience will allow us to explicitly calculate quantities that relate behaviors of traveling waves to model parameters. We now discuss some of our choices for the function form of the transient input $I(x,t)$. We find that systems receiving spatially homogeneous, temporally pulsatile stimuli

$$I(x,t) = I_0\delta(t) \qquad (6)$$

admit mathematical analysis. The intrinsic dynamics of the network (1) exponentially filters this signal so that its effects are spread over the (infinite) window of time following the stimulus. However, spatially localized stimuli such as the square pulse

$$I(x,t) = I_0 H(\Delta_x - |x-x_p|)\delta(t), \qquad (7)$$

with width Δ_x and spatial location x_p, provide more interesting results. In this case, one can consider the effects of perturbing a particular location on a wave. We also consider spatially homogeneous perturbations that last a finite amount of time Δ_t given by

$$I(x,t) = I_0[H(t) - H(t-\Delta_t)], \qquad (8)$$

in the case of traveling fronts.

We now develop a theory for how transient inputs affect the propagation of traveling waves. In particular, perturbation theory is used to approximate the long-time location of the leading edge of a traveling wave.

III. TRAVELING FRONTS IN AN EXCITATORY NEURAL FIELD

The existence and stability of traveling fronts in neural fields is well studied [18–21,26,31,44]. However, there have been very few studies regarding the effects of transient stimuli on them [23,24]. In Ref. [31] it was shown that fronts may lock to moving step-shaped inputs if their amplitude is large enough and the input speed is close enough to the natural wave speed. Recently, the effects of external noise on the speed and variance of traveling fronts have been studied [33,45]. The detailed analysis that we present in this section leads us to several conclusions, which we state now. The long-term consequence of transient inputs is that they effectively shift the location of fronts. We study only progressing fronts and the direction of the shift depends on whether the input is excitatory

or inhibitory. Finally, there is a function that relates the shift of the front to the amplitude and sign of the input, which we approximate.

A. Wave response function: Adjoint

In the absence of inputs ($I(x,t) = 0$), Eq. (1) has a unique traveling front solution $u(x,t) = U(x - ct)$ with speed c, provided [18] (i) $f \in C^1$ and $f'' > 0$, (ii) the function $-u + f(u)$ has only three fixed point $u_0 < u_1 < u_2$ with $u_{0,2}$ stable, and (iii) $w \in C$ is even and a positive function with $\int_{-\infty}^{\infty} w(x)dx < \infty$. Conditions (i) and (ii) are satisfied for the sigmoid firing rate function (4) with finite gain. Even though the Heaviside firing rate function (5) does not satisfy these, the wave front can be calculated explicitly [12,18,20].

Since Eq. (1) possesses a traveling front solution $u(x,t) = U(\xi)$, where $\xi = x - ct$, when $I(x,t) = 0$, we have

$$-cU_\xi = -U + \int_{-\infty}^{\infty} w(\xi - y) f[U(y)]dy. \tag{9}$$

We can consider how transient inputs alter a front using perturbation theory on Eq. (1). Assuming $0 < |I(x,t)| \ll 1$, we rewrite $I(x,t) = \varepsilon J(x,t)$, where $0 < \varepsilon \ll 1$. Changing variables in Eq. (1) from (x,t) to (ξ,t), we have an evolution equation for $u(\xi,t)$ given by

$$-cu_\xi + u_t = -u + \int_{-\infty}^{\infty} w(\xi - y) f[u(y,t)]dy + \varepsilon J(\xi,t). \tag{10}$$

Now, by performing the perturbation expansion

$$u(\xi,t) = U(\xi - \varepsilon v(t)) + \varepsilon u_1(\xi,t) + \varepsilon^2 u_2(\xi,t) + \cdots, \tag{11}$$

where $U(\xi - \varepsilon v(t))$ satisfies Eq. (9) and $\eta(t) = \varepsilon v(t)$ is a small time-dependent shift function. Plugging the expansion (11) into Eq. (10), we find that the first-order term u_1 satisfies the inhomogeneous linear equation

$$-\frac{\partial u_1(\xi,t)}{\partial t} + \mathcal{L}u_1(\xi,t) = -\frac{dv}{dt}U_\xi - J(\xi,t), \tag{12}$$

where $\mathcal{L}$ is the linear operator

$$\mathcal{L}u = c\frac{du}{d\xi} - u + \int_{-\infty}^{\infty} w(\xi - y)\frac{df[U(y)]}{dU}u(y)dy.$$

A bounded solution of Eq. (12) will exist if its right-hand side is orthogonal to all the elements of the null space of the adjoint operator $\mathcal{L}^*$ [18,20]. It is straightforward to calculate the adjoint with respect to the L^2 inner product as

$$\mathcal{L}^*u = -c\frac{du}{d\xi} - u + \frac{df(U)}{dU}\int_{-\infty}^{\infty} w(\xi - y)u(y)dy. \tag{13}$$

It can be proved that $\mathcal{L}^*$ has a one-dimensional null space [18], which is spanned by some function $V(\xi)$. Therefore, Eq. (12) has a bounded solution if

$$\int_{-\infty}^{\infty} \frac{dU}{d\xi}V(\xi)d\xi\frac{dv}{dt} = -\int_{-\infty}^{\infty} J(\xi,t)V(\xi)d\xi.$$

Thus, by isolating the $\frac{dv}{dt}$ term and integrating in time, we find that the shift $\eta = \varepsilon v$ to the traveling front resulting from some small transient input $I = \varepsilon J$ will be

$$\eta(t) = -\frac{\int_{-\infty}^{\infty} V(\xi)\int_0^t I(\xi,s)ds\,d\xi}{\int_{-\infty}^{\infty}\frac{dU}{d\xi}V(\xi)d\xi}, \tag{14}$$

where we have reabsorbed the ε. For temporally pulsatile inputs, we can also calculate η explicitly. In particular, we analyze the case where $f(u) = H(u - \theta)$, since a great deal can be computed directly.

B. Fronts for the Heaviside firing rate

The traveling front solution in the case of a Heaviside firing rate (5) will be superthreshold [$U(\xi) > \theta$] on the infinite domain $\xi \in (-\infty,0)$, crossing threshold at zero so that $U(0) = \theta$. We can choose the threshold crossing point arbitrarily due to the translation invariance of Eq. (1) when $I = 0$. This yields [20]

$$-cU_\xi = -U + \int_{-\infty}^{0} w(\xi - y)dy,$$

which can be solved using an integrating factor [20]

$$U(\xi) = e^{\xi/c}\left(\theta - \frac{1}{c}\int_0^{\xi} e^{-y/c}\int_y^{\infty} w(x)dx\,dy\right). \tag{15}$$

Restricting our study to progressing fronts ($c > 0$), we can require boundedness as $\xi \to \infty$ using the condition on the threshold

$$\theta = \frac{1}{c}\int_0^{\infty} e^{-y/c}\int_y^{\infty} w(x)dx\,dy, \tag{16}$$

so that Eq. (15) becomes

$$U(\xi) = \frac{1}{c}\int_0^{\infty} e^{-y/c}\int_{y+\xi}^{\infty} w(x)dx\,dy. \tag{17}$$

For the exponential weight function (2), the threshold condition (16) becomes $\theta = 1/2(c+1)$, which we can solve explicitly for the front speed

$$c = \frac{1}{2\theta} - 1, \tag{18}$$

where $\theta \in (0,1/2)$ so that $c \in (0,\infty)$. The explicit expression for the traveling front (17), in terms of the threshold θ, will be

$$U(\xi) = \begin{cases} \theta e^{-\xi}, & \xi > 0 \\ 1 - \frac{(1-2\theta)^2}{1-4\theta}e^{2\theta\xi/(1-2\theta)} + \frac{\theta}{1-4\theta}e^{\xi}, & \xi < 0. \end{cases} \tag{19}$$

For illustrative purposes, we plot the front (19) in Fig. 1; pictures for similar models can also be found in Refs. [20,21,27,46]. In particular, the threshold θ of the firing rate function $f(u) = H(u - \theta)$ is denoted in Fig. 1. For some of our calculations regarding the response of traveling fronts to transient stimuli, we pay close attention to the interaction of the field u with the threshold θ.

We now examine the effects different classes of perturbation have upon the location of the traveling front in the coordinate ξ. There has been some recent successful work concerning the effect of periodic and random inhomogeneities on the speed of

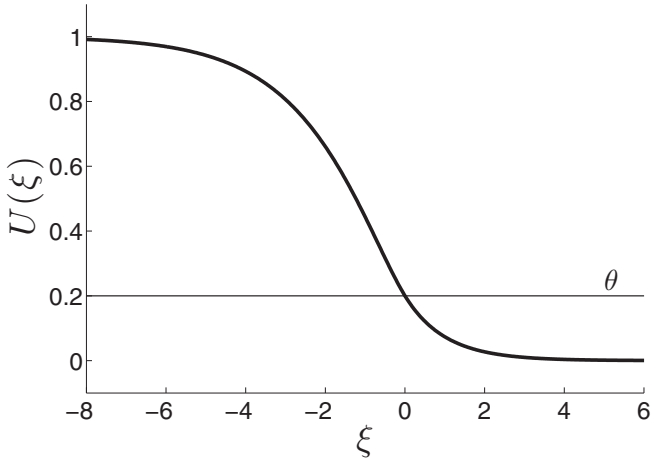

FIG. 1. Profile of the front $U(\xi)$ in the traveling wave coordinate ξ for threshold $\theta = 0.2$ in the scalar neural field (1) with the Heaviside firing rate (5).

the front in neural fields that focuses on the dynamics of front interface [33,47,48]. Our work employs alternative strategies.

C. Spatially homogeneous inputs: Adjoint

To start, we consider the effect of spatially homogenous perturbations on the location of the front in its wave coordinate frame. This allows us to explore the relationship between the amplitude of a transient stimulus and the extent to which the front is shifted. It is straightforward to apply Eq. (14) to find the shift of the wave as it depends upon the stimulus $I(x,t)$, since using the Heaviside firing rate (5) allows us to compute constituent functions analytically. The spatial derivative of the front profile is

$$\frac{dU}{d\xi} = \begin{cases} -\theta e^{-\xi}, & \xi > 0 \\ -\frac{2\theta(1-2\theta)}{1-4\theta} e^{2\theta\xi/(1-2\theta)} + \frac{\theta}{1-4\theta} e^{\xi}, & \xi < 0 \end{cases} \tag{20}$$

and the null space of the adjoint equation (13) is [20]

$$V(\xi) = -H(\xi) e^{-2\theta\xi/(1-2\theta)}. \tag{21}$$

We now plug Eqs. (20) and (21) into our formula (14) for $\eta(t)$ and find that our adjoint approach approximates the response of the front to spatially homogeneous, temporally pulsatile stimuli (6) (such as that shown in Fig. 2) to be

$$\eta(t) = \eta_\infty = \frac{\int_0^\infty e^{-2\theta\xi/(1-2\theta)} I_0 d\xi}{\int_0^\infty e^{-2\theta\xi/(1-2\theta)} (\theta e^{-\xi}) d\xi} = \frac{I_0}{2\theta^2}. \tag{22}$$

Our adjoint approach predicts that the shift to the front scales linearly with the amplitude of spatially homogeneous but temporally pulsatile inputs. We show this prediction along with shifts calculated from numerical simulations in Fig. 3.

In the case of inputs with finite temporal width (8), our perturbative approach predicts

$$\eta(t) = \frac{I_0}{2\theta^2} [\Delta_t + (t - \Delta_t) H(\Delta_t - t)]. \tag{23}$$

Therefore, the shift depends linearly upon the perturbation amplitude and time width. Our adjoint approach generates a linear response function for the transient stimulus's effect on the traveling front, capturing quantitative behavior for sufficiently small perturbations (see Fig. 4). The appearance of the zero-eigenmode solution to the adjoint in our response function should not be surprising, as previous studies of spatially extended systems have employed it to analyze the effects of perturbative inputs [38,49]. However, as we show, we can generate more accurate predictions by examining the interaction of the stimulus with the time-dependent speed of the traveling front.

D. Spatially homogeneous inputs: Speed

We now explore another interpretation of the resulting shift to the front by considering a front, resulting from the perturbation (6), with a time-dependent speed $\psi_t(t)$. We derive this speed using the full nonlinear equation for the speed in terms of a time-dependent threshold $\vartheta(t)$.

To motivate the ansatz we employ to calculate the time-dependent speed, we start by studying Eq. (1) receiving a

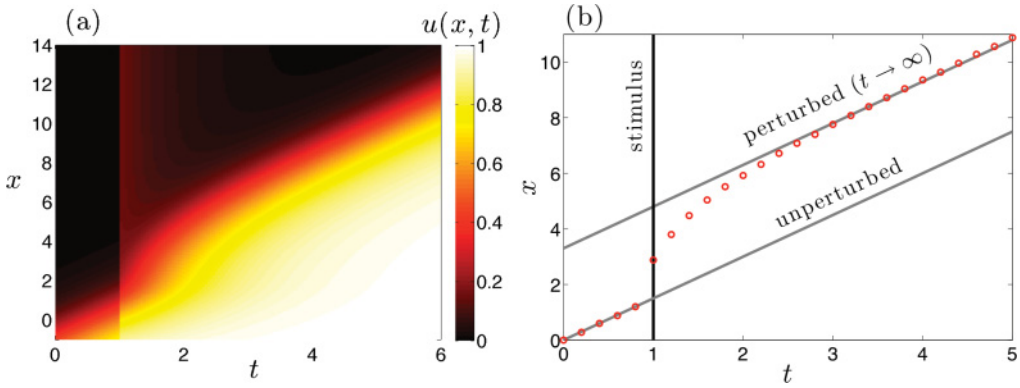

FIG. 2. (Color online) (a) Traveling front in the network (1) with exponential weight (2), Heaviside firing rate (5), and threshold $\theta = 0.2$ ($c = 1.5$) receiving a spatially homogeneous, temporally pulsatile stimulus (6) of amplitude $I_0 = 0.15$. Notice the transient change in the front's shape, which eventually returns to the translationally invariant but advanced front. (b) Comparison of the perturbed front's interface $u(x,t) = \theta$ to the unperturbed front's. Equation (1) was numerically solved using a fourth-order Runge-Kutta method with $dt = 0.001$ and Simpson's rule for the convolution with $dx = 0.01$ and free boundaries.

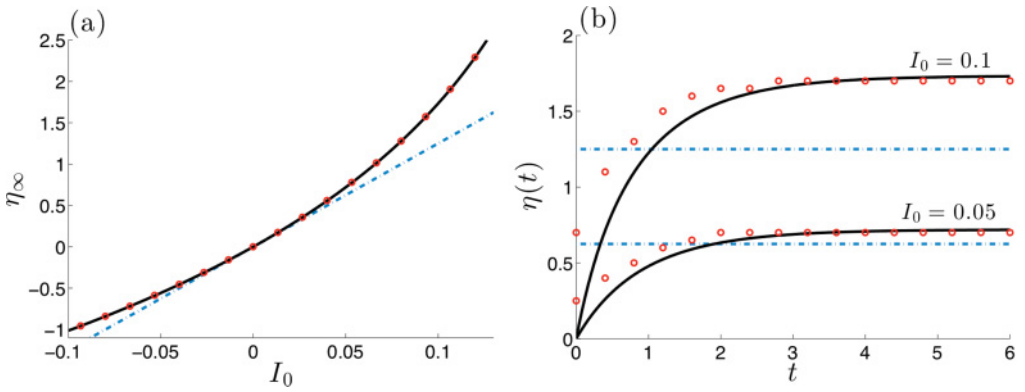

FIG. 3. (Color online) Wave response function η predicted for the spatially homogeneous pulsatile input (6). Shift's (a) long-time behavior η_∞ and (b) time dependence $\eta(t)$ as predicted by the adjoint (22) (dot-dashed line), time-dependent speed (36) (solid line), and numerical simulations (circles). The threshold $\theta = 0.2$, so speed $c = 1.5$. The numerical method is described in Fig. 2.

perturbation (6) when $u(x,t) = 0$ for $t < 0$. When the firing rate is the Heaviside function (5) and $I_0 < \theta$, we have

$$u_t = -u + H(u-\theta)\int_{-\infty}^{\infty} w(x-y)dy + I_0\delta(t),$$

which reduces to

$$u_t = -u + I_0\delta(t), \tag{24}$$

since $H(I_0 - \theta) = 0$ and $u(x,t) \leqslant I_0$. Notice that Eq. (24) is equivalent to Eq. (1) linearized about $u = 0$ with the initial condition $u(x,0) = I_0$. The solution to Eq. (24) is $u = I_0 H(t)e^{\lambda t}$, where $\lambda = -1$, the nonzero eigenvalue of the linearization of Eq. (1).

With this in mind, we will assume that when a traveling front solution to Eq. (1) is perturbed by Eq. (6), the resulting dynamics evolves as

$$u(x,t) = U(\zeta) + I_0 H(t)e^{-t}, \quad \zeta = x - \psi(t), \tag{25}$$

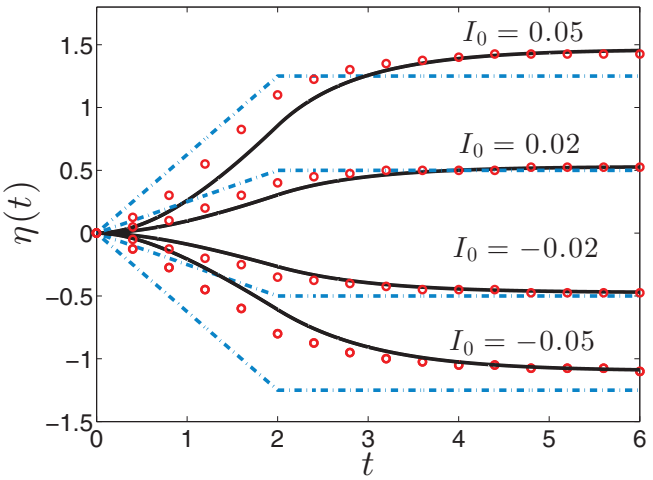

FIG. 4. (Color online) Wave response function $\eta(t)$ for the front (19) perturbed by the spatially homogeneous, temporally finite input (8) calculated using the adjoint (23) (dot-dashed line), time-dependent speed (38) (solid), and from numerical simulations (circles). The threshold $\theta = 0.2$ here, so speed $c = 1.5$. The numerical method is described in Fig. 2.

where $\psi(t)$ may be nonlinear. We find that the time derivative of Eq. (25) is

$$\frac{\partial u(x,t)}{\partial t} = -\frac{d\psi}{dt}U_\zeta + I_0[\delta(t) - H(t)e^{-t}]. \tag{26}$$

Thus, plugging the expression (25) into the evolution equation (1) yields

$$-\frac{d\psi}{dt}U_\zeta + I_0[\delta(t) - H(t)e^{-t}] = -U - I_0 H(t)e^{-t} + \int_{-\infty}^{\infty} w(\zeta - y)H(U(y) + I_0 H(t)e^{-t} - \theta)dy + I_0\delta(t) \tag{27}$$

for $f(u) = H(u-\theta)$. Thus the ansatz (25) gives us an equation for the modified front solution $U(\zeta)$, once we simplify Eq. (27), to be

$$-\frac{d\psi}{dt}U_\zeta = -U + \int_{-\infty}^{\infty} w(\zeta - y)H(U(y) - \vartheta(t))dy, \tag{28}$$

where

$$\vartheta(t) = \theta - I_0 e^{-t} \tag{29}$$

is a time-dependent threshold. We now break the translation invariance of Eq. (28) by fixing the location of the threshold crossing point at $\zeta = 0$ in the wave coordinate frame, so that

$$-\frac{d\psi}{dt}U_\zeta = -U + \int_{-\infty}^{0} w(\zeta - y)dy. \tag{30}$$

Our analysis now proceeds analogously to the case of constant threshold and speed, carried out in Sec. III B. We solve Eq. (30) explicitly using an integrating factor

$$U(\zeta) = e^{\zeta/\psi_t}\left(\vartheta(t) - \frac{1}{\psi_t}\int_0^{\zeta} e^{-y/\psi_t}\int_y^{\infty} w(x)dx\,dy\right). \tag{31}$$

For progressing fronts ($\psi_t > 0$), boundedness can be ensured with the time-dependent threshold condition

$$\vartheta(t) = \frac{1}{\psi_t}\int_0^{\infty} e^{-y/\psi_t}\int_y^{\infty} w(x)dx\,dy. \tag{32}$$

For the exponential weight function (2), we can evaluate the threshold condition (32) to find a nonlinear relationship between the time-dependent speed $\psi_t(t)$ and the time-dependent threshold $\vartheta(t)$ given by

$$\frac{1}{2[\psi_t(t)+1]} = \vartheta(t) = \theta - I_0 e^{-t}. \tag{33}$$

We can isolate the time-dependent wave speed in Eq. (33) to find

$$\psi_t(t) = \frac{1}{2(\theta - I_0 e^{-t})} - 1, \tag{34}$$

where we require $\theta \in (0,1/2)$ and $\theta - I_0 \in (0,1/2)$, so that $\psi_t(t) \in (0,\infty)$. Subtracting the unperturbed front's speed c, given by Eq. (18), from this expression gives us the difference between the time-dependent perturbed wave's speed and the unperturbed wave's

$$\psi_t(t) - c = \frac{I_0 e^{-t}}{2\theta(\theta - I_0 e^{-t})}. \tag{35}$$

To compute the amount of shift a front will undergo following the spatially homogenous perturbation, we need to integrate this difference (35) with respect to time

$$\eta(t) = \int_0^t [\psi_s(s) - c]ds = \int_0^t \frac{I_0 e^{-s}}{2\theta(\theta - I_0 e^{-s})} ds = \frac{1}{2\theta} \ln\left[\frac{\theta - I_0 e^{-t}}{\theta - I_0}\right]. \tag{36}$$

The nonlinear time-dependent speed calculation approximates the shift of the front much better because it considers effects of the input that are of higher order than those of the adjoint approximation (Fig. 3). To more accurately capture the effects of the input, one must perturb about the front with speed $\psi(t)$ given by Eq. (34).

Notice that by taking the limit of Eq. (36) as $t \to \infty$ and Taylor expanding in I_0, we have

$$\eta_\infty = \frac{1}{2\theta} \ln \frac{\theta}{\theta - I_0} = \frac{I_0}{2\theta} + \frac{I_0^2}{4\theta^3} + \frac{I_0^3}{6\theta^4} + \cdots. \tag{37}$$

Thus the linear term of the long-time behavior of the shift predicted by our time-dependent speed approximation is exactly that given by the adjoint approximation (22). Essentially, the time-dependent speed approximation (36) improves by taking into account higher-order, time-dependent effects of the spatially homogeneous perturbation, as shown in Fig. 3.

Analyzing the effects of a spatially homogeneous stimulus of finite-time width (8), we can also use this approach. As before, we derive a time-dependent wave speed $\psi_t(t)$ as determined by the time-dependent threshold

$$\vartheta(t) = \begin{cases} \theta - I_0(1 - e^{-t}), & t \in [0,\Delta_t] \\ \theta - I_0(e^{\Delta_t} - 1)e^{-t}, & t \in [\Delta_t,\infty). \end{cases}$$

We use the threshold (38) to calculate the difference between the modified time-dependent speed $\psi(t)$ of the front and the unperturbed wave speed c as

$$\psi_t(t) - c = \begin{cases} \frac{I_0(1-e^{-t})}{2\theta[\theta - I_0(1-e^{-t})]}, & t \in [0,\Delta_t] \\ \frac{I_0(e^{\Delta_t}-1)e^{-t}}{2\theta[\theta - I_0(e^{\Delta_t}-1)e^{-t}]}, & t \in [\Delta_t,\infty). \end{cases}$$

Integrating Eq. (38), we can compute the time-dependent shift

$$\begin{aligned}\eta(t) &= \int_0^t [\psi_s(s) - c]ds \\ &= \int_0^{\min(t,\Delta_t)} \frac{I_0(1-e^{-s})}{2\theta[\theta - I_0(1-e^{-s})]} ds \\ &\quad + \int_{\Delta_t}^{\max(t,\Delta_t)} \frac{I_0(e^{\Delta_t}-1)e^{-s}}{2\theta[\theta - I_0(e^{\Delta_t}-1)e^{-s}]} ds,\end{aligned}$$

and evaluating the integrals yields

$$\begin{aligned}\eta(t) &= \frac{I_0 \min(t,\Delta_t)}{2\theta(\theta - I_0)} \\ &\quad - \frac{1}{2(\theta - I_0)} \ln\left[\frac{\theta}{\theta - I_0(1 - e^{-\min(t,\Delta_t)})}\right] \\ &\quad + \frac{1}{2\theta} \ln\left[\frac{\theta - I_0(e^{\Delta_t} - 1)e^{-\max(t,\Delta_t)}}{\theta - I_0(1 - e^{-\Delta_t})}\right].\end{aligned} \tag{38}$$

Note that in the limit $t \to \infty$, Eq. (38) becomes

$$\eta_\infty = \frac{I_0}{2\theta(\theta - I_0)} \left\{\Delta_t - \ln\left[\frac{\theta}{\theta - I_0(1 - e^{-\Delta_t})}\right]\right\}.$$

This approach captures the time dependence and long-time behavior of the shift slightly better than the adjoint calculation (Fig. 4).

E. Spatially localized inputs: Adjoint

In the case of spatially localized inputs, we can examine the effect of different stimulus locations on the shift of the traveling front. This reveals the true power of our adjoint approach, providing approximations to the resultant shift of the front's location. In fact, this provides us with a picture similar to the idea of a phase response curve (PRC), where phase shift amplitudes depend on the locations of perturbations in the phase of a limit cycle [50]. The adjoint associated with the traveling front solution, in this case $V(\xi)$ given by Eq. (21), acts as a linear filter through which the transient stimulus is passed to determine its effect. The time-dependent speed approximations would be tedious to develop for spatially localized inputs, especially since such inputs would generate multiple interfaces.

To study the front's response to spatially localized inputs, we simply plug the adjoint (21) and the spatial derivative of the front (20) into our wave response function (14). In the case of a spatially localized, pulsatile stimulus (7), we find that this approach approximates the shift to the wave as

$$\eta_\infty = \frac{I_0}{\theta^2} \begin{cases} \exp\left(-\frac{2\theta x_p}{1-2\theta}\right) \sinh \frac{2\theta\Delta_x}{1-2\theta}, & x_p > \Delta_x \\ \frac{1-\exp\left[-\frac{2\theta(x_p+\Delta_x)}{1-2\theta}\right]}{2}, & x_p \in (-\Delta_x,\Delta_x) \\ 0, & x_p < -\Delta_x, \end{cases} \tag{39}$$

so inputs applied solely to the superthreshold region of the front do not shift it at all. We plot this theoretical prediction along with the results of numerical simulations in Fig. 5. By analogy with phase response curves, the wave response function of the traveling front here is type I, since it is non-negative. Only the sign of the perturbation determines the sign of the shift; the spatial location affects only the amplitude of the shift.

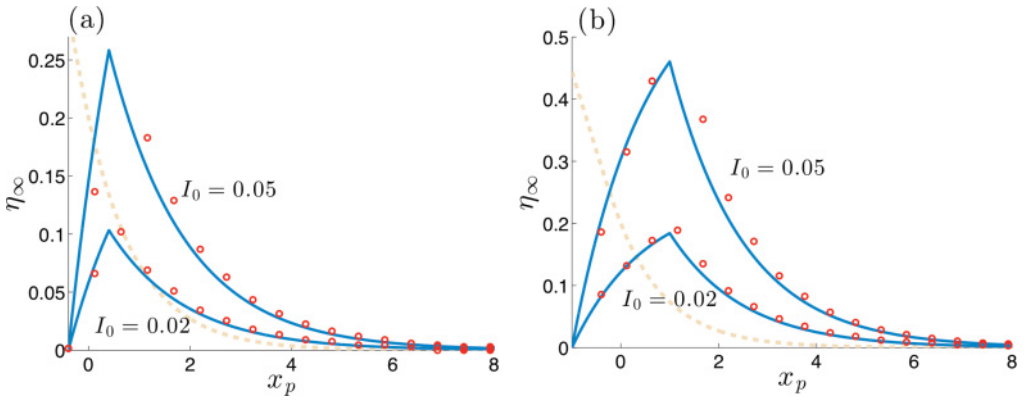

FIG. 5. (Color online) Traveling front's wave response function η_∞ for a spatially localized input (7) for (a) $\Delta_x = 0.4$ and (b) $\Delta_x = 1$, comparing adjoint theory (39) (line) to numerical simulations (circles). The associated front (19) is also plotted, when $\theta = 0.2$ (dashed line). The numerical method is described in Fig. 2.

This is consistent with the positivity of the exponential weight function (2). Notice also that as the width of the stimulus is increased, the peak of the wave response function shifts rightward. In our study of traveling pulses, we will find that the sign of the wave response function can depend on the spatial location of perturbations.

IV. TRAVELING PULSES IN A LATERAL INHIBITORY NEURAL FIELD

We now study the effects of transient inputs on traveling pulses in Eq. (1) with an asymmetric weight kernel (3) for $l = \pi$. The existence and stability of traveling pulse solutions in neural fields are well studied [21,27,46] along with the effects of periodic inhomogeneities on their speed [51]. However, there has yet to be a substantial study of transient inputs on their behavior. Recently, the effect of spatial inhomogeneities in parameters was considered as a model of epileptic tissue [52]. Conceivably, the traveling pulses generated by regions of cortex prone to seizures could be controlled by some transient input to reduce pathological effects of such rogue activity [53].

Here we find that the effect of stimuli on pulse solutions can be more intricate than upon fronts. This comes from lateral inhibition we introduce and the fact that a pulse has both a front and back. The two interfaces of the wave afford more opportunity for small perturbations to have considerable effects. Neural field models that generate traveling pulse solutions usually require a recovery variable [21,26,29,46]. Here we consider a coupling asymmetry with lateral inhibition [40]. This leads to more complicated dynamics than fields that support only fronts, even though the evolution equations are still scalar.

A. Wave response function: Adjoint

For a model of a neuronal network with traveling pulses, we employ a neural field with asymmetric coupling [$w(x) \neq w(-x)$]. Asymmetric coupling has been studied before as a model of direction selectivity [40] and a unidirectional circuit for the spread of synchrony [52]. Studying Eq. (1) in the absence of inputs [$I(x,t) = 0$], we now consider traveling pulse solutions. There are no general results for the existence of traveling pulses with smooth nonlinearities, but pulses can be explicitly calculated with the Heaviside nonlinearity [54]. Supposing the network supports a traveling pulse with speed c, then $u(x,t) = U(\xi)$, where $\xi = x - ct$, the traveling wave coordinate, and $U(\pi) = U(-\pi)$. Plugging this into Eq. (1), we have

$$-cU_\xi = -U + \int_{-\pi}^{\pi} w(\xi - y) f[U(y)] dy. \tag{40}$$

Notice that this is the same as Eq. (9) up to assumptions regarding the form of $U(\xi)$, $w(\xi)$, and the domain. In fact, if we consider the alterations that transient inputs to Eq. (1) will have upon the corresponding traveling pulse solution, the form of the shift η to the wave is derived in the same way it was in the case of fronts. Therefore, to first order, the shifted pulse evolves in time as $U(\xi - \eta(t))$, where the shift $\eta(t)$ is given by

$$\eta(t) = -\frac{\int_{-\pi}^{\pi} V(\xi) \int_0^t I(\xi,s) ds\, d\xi}{\int_{-\pi}^{\pi} \frac{dU(\xi)}{d\xi} V(\xi) d\xi}, \tag{41}$$

where $V(\xi)$ is the null space of the adjoint operator

$$\mathcal{L}^* u = -c\frac{du}{d\xi} - u + \frac{df(U)}{dU} \int_{-\pi}^{\pi} w(y - \xi) u(y) dy. \tag{42}$$

The adjoint operator $\mathcal{L}^*$ has a similar form to the traveling front case except for the assumptions made upon the functions involved. The traveling wave $U(\xi)$ is now a pulse and the weight function $w(\xi)$ is now asymmetric and includes lateral inhibition.

B. Pulses for the Heaviside firing rate

For simplicity, we now consider traveling pulses in an asymmetric ring model with a Heaviside firing rate (5). In the case of a symmetric kernel, the model has been used to describe orientation tuning in the visual cortex [25]. Note that a similar model was studied previously in Ref. [40], as a representation of a directionally selective network. Traveling pulse solutions $u(x,t) = U(\xi)$ to Eq. (1) with weight (3) and $l = \pi$ will have

superthreshold region of width Δ, which we choose to lie at the rightmost edge of the domain $\xi \in (\pi-\Delta,\pi)$, such that

$$-cU_\xi = -U + A\int_{\pi-\Delta}^{\pi} \cos(\xi - y - \phi)dy. \quad (43)$$

Solving Eq. (43) with an integrating factor, we find

$$U(\xi) = \frac{2\sin\left(\frac{\Delta}{2}\right)\left[c\sin\left(\xi+\frac{\Delta}{2}-\phi\right)-\cos\left(\xi+\frac{\Delta}{2}-\phi\right)\right]}{c^2+1}. \quad (44)$$

Applying the threshold conditions $U(\pi-\Delta)=U(\pi)=\theta$, we can use Eq. (44) to generate a solvable set of equations for the wave speed c and pulse width Δ given by

$$\frac{2A\sin\left(\frac{\Delta}{2}\right)\left[\cos\left(\frac{\Delta}{2}-\phi\right)-c\sin\left(\frac{\Delta}{2}-\phi\right)\right]}{c^2+1} = \theta, \quad (45)$$

$$\frac{2A\sin\left(\frac{\Delta}{2}\right)\left[\cos\left(\frac{\Delta}{2}+\phi\right)+c\sin\left(\frac{\Delta}{2}+\phi\right)\right]}{c^2+1} = \theta. \quad (46)$$

Upon subtracting Eq. (45) from Eq. (46), we find

$$\frac{2A(\cos\Delta-1)}{c^2+1}(\sin\phi - c\cos\phi) = 0.$$

Excluding the solution $\cos\Delta = 1$, by noting that this will not solve the two constituent equations, we find that $c=\tan\phi$ will be the wave speed. Now, adding Eqs. (45) and (46),

$$\frac{2A\sin\Delta(\cos\phi + c\sin\phi)}{c^2+1} = 2\theta,$$

we have an equation for the pulse width Δ in terms of the parameters

$$\sin\Delta = \frac{\theta(c^2+1)}{A(\cos\phi + c\sin\phi)} = \frac{\theta}{A\cos\phi},$$

so there are two pulse widths given on a restricted domain

$$\Delta = \Delta_u = \sin^{-1}[(\theta/A)\sec\phi] \quad \text{(narrow)}$$
$$\Delta = \Delta_s = \pi - \sin^{-1}[(\theta/A)\sec\phi] \quad \text{(wide)}$$

for $\phi \in [0,|\cos^{-1}(\theta/A)|]$. Upon plugging in the expression for c and simplifying using trigonometric identities

$$U(\xi) = A\cos\phi(\sin\xi - \sin(\xi+\Delta)). \quad (47)$$

We plot both existing pulses in Fig. 6(a). The linear stability of the traveling pulses could be computed using Evans functions [44,55]. For brevity, we note that in numerical simulations we observe that the wider pulse is stable Δ_s and the narrow pulse is unstable Δ_u, forming a separatrix between the rest state and the stable pulse. We depict the dependence of the pulse width upon the asymmetry ϕ of the weight kernel in Fig. 6(b), showing that the two pulse branches terminate at a saddle-node bifurcation for a critical value of ϕ.

C. Spatially localized inputs

We now consider the effect of a spatially localized, pulsatile stimulus

$$I(x,t) = H(\Delta_x - |x-x_p|)\delta(t), \quad x\in(-\pi,\pi), \quad (48)$$

on the traveling pulse solution (47). Interestingly, since the spatial domain is periodic, we arrive at a picture more similar to the PRC of a limit cycle oscillator than in the front case. In contrast to excitatory neural fields, where the shift is always the same sign as the stimulus, waves in networks with excitation and inhibition can be shifted positively or negatively with a positive stimulus. To employ our wave response function (41), we first compute the spatial derivative of the pulse solution

$$\frac{dU}{d\xi} = A\cos\phi[\cos\xi - \cos(\xi+\Delta)].$$

Plugging the Heaviside firing rate (5), asymmetric cosine weight (3), and traveling pulse (47) functions into the null equation of the adjoint (42), we have the system

$$cV_\xi + V = C(-\pi)\delta(\xi+\pi) + C(\pi-\Delta)\delta(\xi-\pi+\Delta),$$
$$C(\xi) = \frac{A}{|U'(\pi)|}\int_{-\pi}^{\pi}\cos(y-\xi-\phi)V(y)dy,$$

which allows us to compute the null space $V(\xi)$ of the adjoint operator (42). The homogeneous version of the left-hand side

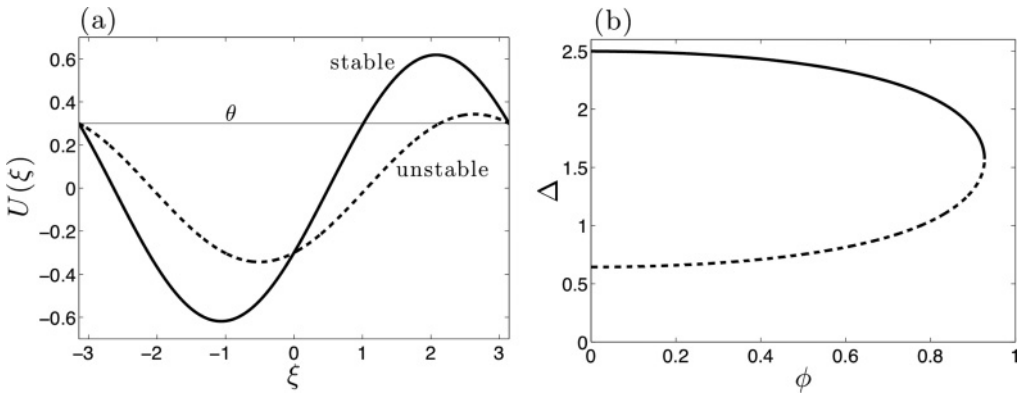

FIG. 6. (a) Stable traveling pulse solution of the neural field (1) with asymmetric weight (3), separated from the rest state $u=0$ by the unstable traveling pulse solution (separatrix) for $\phi=\pi/4$. (b) Widths Δ of stable (solid line) and unstable (dashed line) traveling pulse solutions corresponding to a given level of weight asymmetry ϕ. Other parameters are $\theta=0.3$ and $A=0.5$.

has solutions of the form $Be^{-\xi/c}$. Along with the δ functions on the right-hand side and the 2π periodicity, this suggests a solution of the form

$$V(\xi) = [H(\xi+\pi) + e^{-2\pi/c} + e^{-4\pi/c} + \cdots]e^{-(\pi+\xi)/c} + \alpha[H(\xi-\pi+\Delta) + e^{-2\pi/c} + e^{-4\pi/c} + \cdots] \times e^{(\pi-\Delta-\xi)/c}.$$

The two infinite series arise from the fact that exponential functions originating at $\xi = \pi - \Delta$ and $\xi = -\pi$, in effect, wrap around the domain indefinitely due to periodicity. Plugging this into our adjoint equation, we can self-consistently determine the constant α. We make use of the geometric sum

$$\sum_{n=1}^{\infty} e^{-2n\pi/c} = \frac{1}{2}\left[\coth\left(\frac{\pi}{c}\right) - 1\right].$$

After a straightforward calculation, we find

$$[c - C(-\pi)]\delta(\xi+\pi) + [\alpha c - C(\pi-\Delta)]\delta(\xi+\pi-\Delta) = 0,$$

where

$$C(-\pi) = \frac{c}{1-\cos\Delta}(1+\alpha\cos\Delta)$$

and

$$C(\pi-\Delta) = \frac{c}{1-\cos\Delta}(\cos\Delta+\alpha).$$

Requiring self-consistency, we find $\alpha = -1$, so that

$$V(\xi) = \left[H(\xi+\pi) + \frac{\coth(\pi/c)-1}{2}\right]e^{-(\pi+\xi)/c} - \left[H(\xi+\Delta-\pi) + \frac{\coth(\pi/c)-1}{2}\right]e^{(\pi-\Delta-\xi)/c}.$$

Now we have a periodic, albeit discontinuous, response function that takes on both positive and negative values.

Notice that for homogeneous inputs $I(x,t) = I_0\delta(t)$,

$$\eta_\infty = -\frac{I_0\int_{-\pi}^{\pi} V(\xi)d\xi}{\int_{-\pi}^{\pi}\frac{dU(\xi)}{d\xi}V(\xi)d\xi} = 0, \tag{49}$$

so there is no predicted shift. However, when we consider spatially localized pulsatile stimuli (48), our adjoint approach approximates the response function (41) of the pulse as

$$\eta_\infty = -I_0\frac{\mathcal{P}_+(x_p) - \mathcal{P}_-(x_p)}{2A\cos^3\phi(\cos\Delta - 1)} \tag{50}$$

for the piecewise-defined functions

$$\mathcal{P}_+(x_p) = \begin{cases} \mathcal{H}_+ e^{-(\pi+x_p)/c}, & x_p > \Delta_x - \pi \\ \mathcal{H}_- e^{-(\pi+x_p)/c} + \mathcal{E}(-\pi), & x_p < \Delta_x - \pi \end{cases}$$

and

$$\mathcal{P}_-(x_p) = \begin{cases} \mathcal{H}_+ e^{(\pi-\Delta-x_p)/c}, & x_p > p_+ \\ \mathcal{H}_- e^{(\pi-\Delta-x_p)/c} + \mathcal{E}(\pi-\Delta), & x_p \in (p_-, p_+) \\ \mathcal{H}_- e^{(\pi-\Delta-x_p)/c}, & x_p < p_-, \end{cases}$$

where we denote the domain points $p_\pm = \pi - \Delta \pm \Delta_x$ and define the functions

$$\mathcal{H}_\pm = \left[\coth\left(\frac{\pi}{c}\right) \pm 1\right]\sinh\left(\frac{\Delta_x}{c}\right),$$
$$\mathcal{E}(\xi) = 1 - e^{(\xi - x_p - \Delta_x)/c}.$$

Note that we also exclude the case of wide stimuli, so that $2\Delta_x < \Delta$ and $2\Delta_x < \pi - \Delta$. A scaled version of the wave response function (50) is plotted in Fig. 7 along with the stable traveling pulse solution. Stimuli that arrive at the front (back) of the pulse first will advance (delay) the pulse. Notice that this matches the results from numerical simulations very well.

As opposed to the case of the traveling front in an excitatory network, the wave response function of the traveling pulse in the asymmetric ring network changes sign. Thus, excitatory inputs may advance or delay the input depending on their spatial location. Here we point out an analogy between our wave response function and the PRC of limit cycle oscillators derived from spiking neuron models [50,56]. Categorization of PRCs identifies them as either type I, where positive stimuli only advance the phase, or type II, where an advance or delay of the phase can occur. By analogy, our wave response functions seem to be type II for pulses in networks with inhibition and type I otherwise, as in the case of fronts. In a related

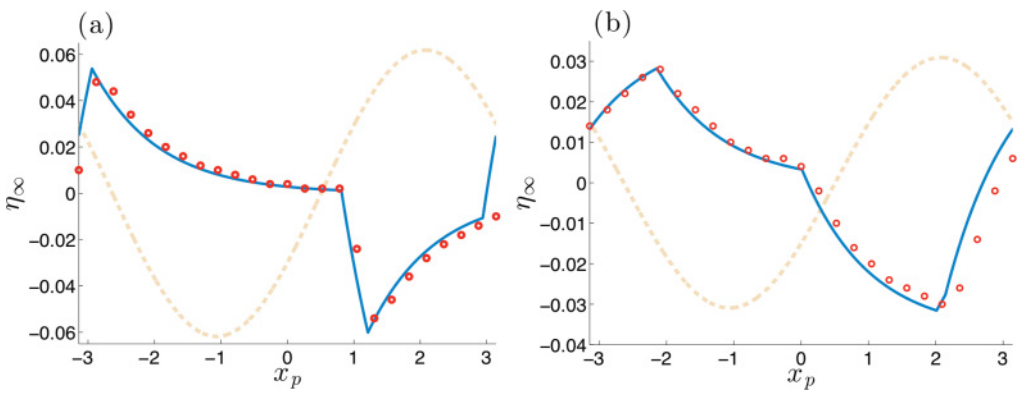

FIG. 7. (Color online) Wave response function η_∞ for a traveling pulse in an asymmetric neural field computed using adjoint theory (50) (solid line) and numerical simulations (circles). The input is Eq. (48) with the parameters (a) $I_0 = 0.1$, $\Delta_x = 0.2$ and (b) $I_0 = 0.02$, $\Delta_x = 1$. The scaled profile of the associated pulse (47) (dashed line) is plotted for the parameters $\theta = 0.3$, $A = 0.5$, and $\phi = \frac{\pi}{4}$. Equation (1) is numerically solved using a fourth-order Runge-Kutta method with $dt = 0.01$ and Simpson's rule for the convolution with $dx = 0.01$ and periodic boundaries.

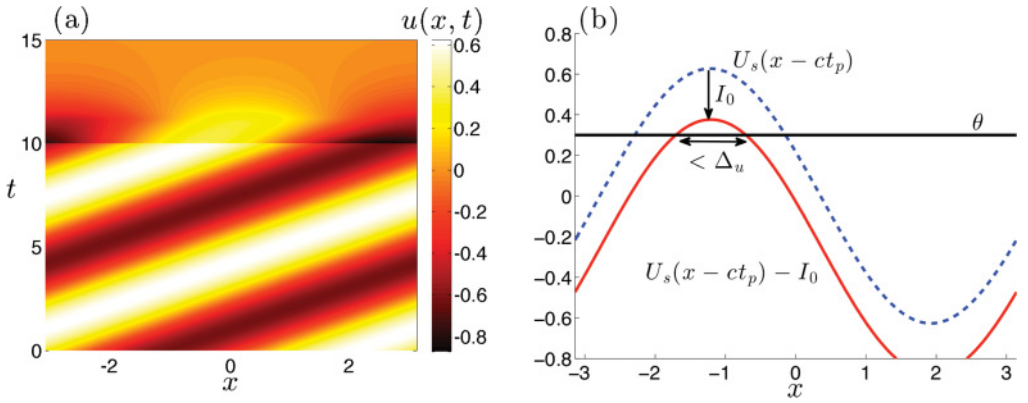

FIG. 8. (Color online) Traveling pulse (47) terminated by a spatially homogeneous pulsatile stimulus $I(x,t) = -I_0\delta(t-t_p)$. (a) Numerical simulation of the asymmetric ring neural field $u(x,t)$ stimulated at $t_p = 10$ with amplitude large enough to terminate the pulse $I_0 > I_0^*$. Other parameters are $\theta = 0.3$, $A = 0.5$, and $\phi = \pi/4$. (b) Illustration of the instantaneous effect of a pulsatile stimulus on the profile of the stable traveling pulse $U_s(\xi)$, where its new width is less than the unstable traveling pulse's width Δ_u. The numerical method is described in Fig. 7.

context, using a nonlinear Fokker-Planck equation, Kawamura *et al.* [39] recently found that the bifurcation structure of a coupled oscillator population determined whether its sensitivity function was type I or type II.

D. Terminating pulses

To this point, we have considered how transient stimuli elicit perturbative changes to the structure of traveling waves. We now study how transient stimuli may serve to terminate traveling pulses, so that the structure of the pulse is permanently altered and the system settles into a rest state [see Fig. 8(a)]. For a spatially homogeneous, pulsatile stimulus, $I(x,t) = -I_0\delta(t)$ (note negativity), we consider the fact that the unstable traveling pulse is a separatrix of the underlying dynamical system (1). Recall that Eq. (49) shows that small perturbations by such a stimulus do not shift the location of the wave. However, transiently forcing the stable propagating pulse strongly enough, so that it has a width smaller than the separatrix's width, may cause the structure to collapse to the rest state.

This motivates us to look for solutions to the equation $U_s(\xi_I) = U_s(\xi_I + \Delta_u)$, where U_s is the stable traveling pulse and Δ_u is the unstable traveling pulse width [see Fig. 8(b)]. To solve for ξ_I, we first express the stable traveling pulse in terms of free parameters by plugging in the width $\Delta_s = \pi - \sin^{-1}[(\theta/A)\sec\phi]$ to yield

$$U_s(\xi) = A\cos\phi(\sin\xi + \sin\{\xi - \sin^{-1}[(\theta/A)\sec\phi]\}).$$

Then, simplifying the equation $U(\xi_I) = U(\xi_I + \Delta_u)$ yields

$$\begin{aligned}\sin\{\xi_I - \sin^{-1}[(\theta/A)\sec\phi]\} &= \sin\{\xi_I + \sin^{-1}[(\theta/A)\sec\phi]\},\\ \pi - \xi_I + \sin^{-1}[(\theta/A)\sec\phi] &= \xi_I + \sin^{-1}[(\theta/A)\sec\phi],\\ \xi_I &= \frac{\pi}{2}.\end{aligned}$$

Therefore, the associated value of U_s is

$$\begin{aligned}U_s\left(\frac{\pi}{2}\right) &= A\cos\phi(\cos\{\sin^{-1}[(\theta/A)\sec\phi]\} + 1)\\ &= A\cos\phi\left(\sqrt{1-\frac{\theta^2}{A\cos^2\phi}} + 1\right).\end{aligned}$$

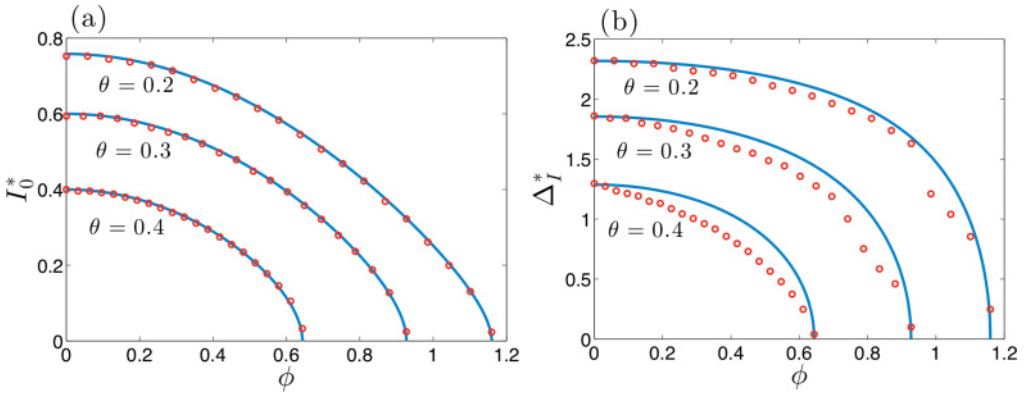

FIG. 9. (Color online) (a) Critical terminating stimulus amplitude I_0^* predicted based on separatrix theory (51) (line) and computed with numerical simulations (circles) for various threshold θ values. (b) Critical terminating stimulus width Δ_I^* predicted by Eq. (53) (line) and computed using numerical simulations (circles) for various threshold θ values. We assume here that the amplitude of the stimulus satisfies the inequality (52). The weight amplitude $A = 0.5$. The numerical method is described in Fig. 7.

This indicates that the minimal spatially homogeneous stimulus amplitude I_0^* required to shut off a traveling pulse is given by the equation $\theta = U_s(\pi/2) - I_0^*$, so

$$I_0^* = A\cos\phi\left(\sqrt{1-\frac{\theta^2}{A^2\cos^2\phi}}+1\right)-\theta. \qquad (51)$$

We plot this along with numerically determined critical stimulus amplitudes in Fig. 9(a). As the parameter ϕ is increased to the saddle-node bifurcation point, the critical stimulus amplitude needed to terminate the pulse decreases toward zero.

An alternative paradigm for transient stimuli considers a long but finite forcing of the network. Presuming that the stimulus lasts longer than the relaxation time of the neural field, we can think of shutting off the stable traveling pulse by in effect sliding it off the stable branch of pulses, past the saddle-node bifurcation in parameter space. Therefore, the effective threshold of the network simply has to be higher than the threshold value of the saddle-node bifurcation $\theta_{\rm SN} = A\cos\phi$. Therefore, a long but transient stimulus could kill a pulse if its amplitude $I_0 + \theta > \theta_{\rm SN}$ or, equivalently, $I_0 > A\cos\phi - \theta$, as long as it lasts a sufficient amount of time.

For pulsatile stimuli of finite width

$$I(x,t) = -I_0\delta(t)H(\xi - \pi + \Delta_I),$$

at the right edge of the domain, it is only necessary to narrow the pulse below the unstable pulse's width. In particular, if we consider a rectangular region of negative stimulus, its amplitude must exceed the maximal value of U_s and it must be wider than $\Delta_s - \Delta_u$. Thus, as long as the stimulus amplitude satisfies the inequality

$$I_0 > 2A\cos\left\{\frac{\sin^{-1}[(\theta/A)\sec\phi]}{2}\right\}\cos\phi, \qquad (52)$$

then we predict that the critical width of the stimulus to shut off the pulse is

$$\Delta_I^* = \Delta_s - \Delta_u = \pi - 2\sin^{-1}[(\theta/A)\sec\phi]. \qquad (53)$$

We compare this critical stimulus width prediction with the results of numerical simulations in Fig. 9(b). It is assumed that we apply the stimulus in the rightmost region of the domain, but we could make corrections for stimuli applied in front of the pulse or in its interior.

V. CONCLUSION

We have studied the effects of transient inputs on the position of traveling waves in neural fields. Inputs can cause waves to shift in the wave coordinate frame. In particular, we found that using perturbation theory to derive a response function involving the adjoint of the linearized wave equation provides a reasonable approximation for the shift in position. There is a clear analogy between the response function we have derived for waves and the phase response curve of limit cycle oscillators [50]. The strictly non-negative response function we derive for traveling fronts in an excitatory network can be thought of as type I since the sign of the perturbation determines the sign of the wave shift. In contrast, the response function we derive for traveling pulses in a lateral inhibitory network indicates that the spatial position of perturbations can determine the sign of the wave's shift, a type-II property. Since the process of obtaining the wave response function can be generalized, it could be applied to a number of other neural field models. In particular, it would be interesting to see how a negative feedback variable such as a separate inhibitory population [14], spike frequency adaptation [21,29], or synaptic depression [26] would affect the shape of the response function. Adjoints for models with linear recovery have been calculated previously in Ref. [32,51]. Type-II response functions in lateral inhibitory networks may be separable into positive and negative parts in analogous two population networks, depending on whether the excitatory or inhibitory population is stimulated. In addition, spatially structured solutions arising in two-dimensional models such as spiral waves [30] or traveling spots [57] could also be analyzed in this framework. Such an approach may even predict the angle of deflection of moving spots resulting from a transient input [58].

In addition to the derivation using the adjoint, in the case of traveling fronts, a complementary approach was used to calculate the wave response function for spatially homogeneous inputs. By tracking the time-dependent speed of the front, we were able to approximate the long-time behavior of the shift even better. The adjoint method is an exact method that comes from a perturbation expansion of the response of the fronts and pulses to small stimuli. The time-dependent speed method employs an approximation (not a systematic expansion) that contains a mixture of nonlinear and linear estimates. It would be interesting to see if some higher-order approximation of the wave response function could capture the nonlinear dependence of the shift upon perturbation amplitude that the time-dependent speed approach does.

Predictions based on our analysis of the termination of traveling pulses could be linked to experimental studies of epileptiform activity *in vitro* [2,9–11] and *in vivo* [36,59]. Our results provide a theory for the previous experimental finding that large-scale response properties of neural tissue are activity state dependent. In Ref. [10] the initiation of traveling pulses was studied in cortical slices using a stimulating electrode. At a critical amplitude of current stimulation, the probability of an initiation event drastically increased. This suggests it may be necessary for a critical volume of cells to be spiking to initiate a traveling pulse. Thus, once a traveling pulse begins to propagate in a cortical slice, it may be possible to terminate the pulse by ceasing spiking in enough cells so that the population of active cells falls below the critical volume. Negative feedback processes such as spike frequency adaptation or inhibition will likely switch on once the pulse begins to propagate, so this critical volume may be even higher for an already active slice. Termination events were studied in Ref. [10], but they occurred spontaneously, rather than through external electrode stimulation. In Ref. [60] traveling neural activity waves in a culture of neurons were shown to cease when the concentration of an excitatory receptor antagonist was increased beyond a threshold level. This suggests there may also be a critical level of tissue excitability for wave genesis. For the control of epileptiform activity in the brain, a model-based predictive controller will most likely be

necessary [53]. Thus it would be useful to study the problem of terminating traveling pulses in neuronal network models with more details that address the complications of the *in vivo* problem. For example, our analysis could be adapted to noisy neural fields or spiking neuron networks.

ACKNOWLEDGMENTS

Z.P.K. is supported by a National Science Foundation (NSF) Mathematical Sciences Postdoctoral Research Fellowship (Grant No. DMS-1004422). B.E. was supported by the NSF (Grant No. DMS-0817131).

[1] X.-J. Wang, Physiol. Rev. **90**, 1195 (2010).
[2] J.-Y. Wu, Neuroscientist **14**, 487 (2008).
[3] K. R. Delaney, A. Gelperin, M. S. Fee, J. A. Flores, R. Gervais, D. W. Tank, and D. Kleinfeld, Proc. Natl. Acad. Sci. USA **91**, 669 (1994).
[4] F. Han, N. Caporale, and Y. Dan, Neuron **60**, 321 (2008).
[5] W. Xu, X. Huang, K. Takagaki, and J.-Y. Wu, Neuron **55**, 119 (2007).
[6] G. B. Ermentrout and D. Kleinfeld, Neuron **29**, 33 (2001).
[7] D. Rubino, K. A. Robbins, and N. G. Hatsopoulos, Nature Neurosci. **9**, 1549 (2006).
[8] R. J. Morgan and I. Soltesz, Proc. Natl. Acad. Sci. USA **105**, 6179 (2008).
[9] R. D. Chervin, P. A. Pierce, and B. W. Connors, J. Neurophysiol. **60**, 1695 (1988).
[10] D. J. Pinto, S. L. Patrick, W. C. Huang, and B. W. Connors, J. Neurosci. **25**, 8131 (2005).
[11] K. A. Richardson, S. J. Schiff, and B. J. Gluckman, Phys. Rev. Lett. **94**, 028103 (2005).
[12] S. Coombes, Biol. Cybern. **93**, 91 (2005).
[13] P. C. Bressloff, J. Phys. A: Math. Theor. **45**, 033001 (2012).
[14] H. R. Wilson and J. D. Cowan, Biol. Cybern. **13**, 55 (1973).
[15] S. Amari, Biol. Cybern. **27**, 77 (1977).
[16] G. B. Ermentrout and J. D. Cowan, Biol. Cybern. **34**, 137 (1979).
[17] P. C. Bressloff, J. D. Cowan, M. Golubitsky, P. J. Thomas, and M. C. Wiener, Philos. Trans. R. Soc. London, Ser. B **356**, 299 (2001).
[18] G. B. Ermentrout and J. B. McLeod, Proc. R. Soc. Edinburgh, Sect. A **123**, 461 (1993).
[19] M. Idiart and L. Abbott, Network **4**, 285 (1993).
[20] P. C. Bressloff, Physica D **155**, 83 (2001).
[21] D. J. Pinto and G. B. Ermentrout, SIAM J. Appl. Math. **62**, 206 (2001).
[22] C. R. Laing, W. C. Troy, B. Gutkin, and G. B. Ermentrout, SIAM J. Appl. Math. **63**, 62 (2002).
[23] A. Hutt, M. Bestehorn, and T. Wennekers, Network **14**, 351 (2003).
[24] A. Hutt and F. M. Atay, Chaos Solitons Fractals **32**, 547 (2007).
[25] R. Ben-Yishai, D. Hansel, and H. Sompolinsky, J. Comput. Neurosci. **4**, 57 (1997).
[26] Z. P. Kilpatrick and P. C. Bressloff, Physica D **239**, 547 (2010).
[27] W. C. Troy and V. Shusterman, SIAM J. Appl. Dyn. Syst. **6**, 263 (2007).
[28] S. Folias and P. Bressloff, SIAM J. Appl. Dyn. Syst. **3**, 378 (2004).
[29] S. Coombes and M. R. Owen, Phys. Rev. Lett. **94**, 148102 (2005).
[30] C. Laing, SIAM J. Appl. Dyn. Syst. **4**, 588 (2005).
[31] S. E. Folias and P. C. Bressloff, SIAM J. Appl. Math. **65**, 2067 (2005).
[32] G. B. Ermentrout, J. Z. Jalics, and J. E. Rubin, SIAM J. Appl. Math. **70**, 3039 (2010).
[33] S. Coombes and C. R. Laing, Phys. Rev. E **83**, 011912 (2011).
[34] M. Rule, M. Stoffregen, and B. Ermentrout, PLoS Comput. Biol. **7**, e1002158 (2011).
[35] V. A. Billock and B. H. Tsou, Proc. Natl. Acad. Sci. USA **104**, 8490 (2007).
[36] B. J. Gluckman, H. Nguyen, S. L. Weinstein, and S. J. Schiff, J. Neurosci. **21**, 590 (2001).
[37] X. Han, X. Qian, J. G. Bernstein, H.-H. Zhou, G. T. Franzesi, P. Stern, R. T. Bronson, A. M. Graybiel, R. Desimone, and E. S. Boyden, Neuron **62**, 191 (2009).
[38] A. Mikhailov, L. Schimansky-Geier, and W. Ebeling, Phys. Lett. **96A**, 453 (1983).
[39] Y. Kawamura, H. Nakao, and Y. Kuramoto, Phys. Rev. E **84**, 046211 (2011).
[40] X. Xie and M. A. Giese, Phys. Rev. E **65**, 051904 (2002).
[41] H. Suarez, C. Koch, and R. Douglas, J. Neurosci. **15**, 6700 (1995).
[42] A. J. Watt, H. Cuntz, M. Mori, Z. Nusser, P. J. Sjostrom, and M. Hausser, Nature Neurosci. **12**, 463 (2009).
[43] H. V. Oviedo, I. Bureau, K. Svoboda, and A. M. Zador, Nature Neurosci. **13**, 1413 (2010).
[44] S. Coombes and M. R. Owen, SIAM J. Appl. Dyn. Syst. **3**, 574 (2004).
[45] P. C. Bressloff and M. A. Webber (unpublished).
[46] S. Coombes, G. J. Lord, and M. R. Owen, Physica D **178**, 219 (2003).
[47] S. Coombes, C. R. Laing, H. Schmidt, N. Svanstedt, and J. A. Wyller, Discrete Cont. Dyn. Syst. Ser. A (to be published).
[48] H. Schmidt, A. Hutt, and L. Schimansky-Geier, Physica D **238**, 1101 (2009).
[49] Y. Kawamura, H. Nakao, K. Arai, H. Kori, and Y. Kuramoto, Phys. Rev. Lett. **101**, 024101 (2008).
[50] B. Ermentrout, Neural Comput. **8**, 979 (1996).
[51] Z. P. Kilpatrick, S. E. Folias, and P. C. Bressloff, SIAM J. Appl. Dyn. Syst. **7**, 161 (2008).
[52] W. C. Troy, SIAM J. Appl. Dyn. Syst. **7**, 1247 (2008).
[53] M. Kamrunnahar, N. S. Dias, and S. J. Schiff, Ann. Biomed. Eng. **39**, 1482 (2011).
[54] D. J. Pinto, R. K. Jackson, and C. E. Wayne, SIAM J. Appl. Dyn. Syst. **4**, 954 (2005).
[55] L. Zhang, J. Diff. Eq. **197**, 162 (2004).
[56] D. Hansel, G. Mato, and C. Meunier, Neural Comput. **7**, 307 (1995).
[57] S. Coombes and M. R. Owen, in *Fluids and Waves: Recent Trends in Applied Analysis*, edited by F. Botelho, T. Hagen, and J. Jamison, AMS Contemporary Mathematics, Vol. 440 (AMS, Providence, RI, 2007), pp. 123–144.
[58] Y. Lu, Y. Sato, and S.-I. Amari, Neural Comput. **23**, 1248 (2011).
[59] V. Shusterman and W. C. Troy, Phys. Rev. E **77**, 061911 (2008).
[60] O. Feinerman, M. Segal, and E. Moses, J. Neurophysiol. **94**, 3406 (2005).